polysaccharides

MDPI

Article

Structural Features of Bacterial Nanocellulose Synthesized on Enzymatic Hydrolyzates of *Miscanthus* × *giganteus*

Evgenia K. Gladysheva [1,*], Vera V. Budaeva [1,*], Anastasia A. Zenkova [1], Ekaterina A. Skiba [1], Ekaterina I. Kashcheyeva [1], Olga V. Tokko [2] and Lyudmila A. Aleshina [2]

[1] Bioconversion Laboratory, Institute for Problems of Chemical and Energetic Technologies, Siberian Branch of the Russian Academy of Sciences (IPCET SB RAS), Biysk 659322, Russia; zenkova_nastasya080401@mail.ru (A.A.Z.); eas08988@mail.ru (E.A.S.); makarova@ipcet.ru (E.I.K.)

[2] Department of Solid State Physics, Institute of Physics and Technology, Petrozavodsk State University, Petrozavodsk 185910, Russia; solvak@yandex.ru (O.V.T.); alkftt@mail.ru (L.A.A.)

* Correspondence: evg-gladysheva@yandex.ru (E.K.G.); budaeva@ipcet.ru (V.V.B.)

Abstract

Bacterial nanocellulose (BNC) is a promising polysaccharide whose properties depend on the supramolecular structure of its crystalline component. The search for cost-effective alternative nutrient media for BNC production requires a deep understanding of how their composition affects the structure. This study aimed to investigate the structural features of BNC synthesized by the symbiotic culture SCOBY on enzymatic hydrolyzates prepared from chemically treated *Miscanthus* × *giganteus* (cv. KAMIS) in comparison with BNC synthesized on a control medium. The study methodology relies on X-ray diffraction analysis performed in reflection and transmission geometries using a full-profile analysis (the Rietveld method) to determine the unit cell parameters and angles, coherent scattering domain (CSD) sizes, and degree of crystallinity (DC). The main results showed that all five BNC samples were identified as Iα cellulose with a content of 95–100% and identical unit cell parameters. The CSD sizes in the reflection and transmission geometries varied in the range of 4.0–7.7 nm, and the longitudinal size was between 12.1 and 18.1 nm. The BNC samples obtained on hydrolyzates exhibited a higher DC (85, 83, 82 and 84%) compared with BNC synthesized on the control medium (78%). It was established that the crystallites of the five BNC samples exhibit anisotropy: the T/R ratio varied from 0.76 to 1.46, depending on the crystallographic direction. The scientific novelty of this work lies in the results of a comprehensive systematic study of the structural features of BNC samples synthesized on miscanthus enzymatic hydrolyzates. It was shown for the first time that replacing the control medium with hydrolyzates improves the BNC quality, which in turn enhances the practical significance of alternative nutrient media. The topic of the cost reduction in the nutrient medium for BNC biosynthesis remains debatable, but this direction aligns with the global trend.

Keywords: bacterial nanocellulose; X-ray diffraction analysis; cellulose Iα; crystallinity; crystallite size

Academic Editor: Tamilselvan Mohan

Received: 2 October 2026
Revised: 27 October 2026
Accepted: 1 November 2026
Published: 3 November 2026

Copyright: © 2026 by the authors. Licensee MDPI, Basel, Switzerland. This article is an open access article distributed under the terms and conditions of the Creative Commons Attribution (CC BY) license.

1. Introduction

Bacterial nanocellulose (BNC) is an extracellular polysaccharide, which is produced by bacteria of the species *Komagataeibacter*, *Acetobacter*, and *Gluconacetobacter* as a biofilm

and composed of glucose units linked via β-1,4-glycosidic bonds [1,2]. During the biosynthesis process, BNC molecules are initially produced intracellularly and subsequently secreted through a series of precisely arranged pores that are present along the longitudinal axis of the bacteria [3]. BNC fibers have a diameter ranging from 10 to 100 nm and are capable of forming a precise three-dimensional network. BNC is characterized by high crystallinity and degree of polymerization, high purity, excellent mechanical properties, and high water-holding capacity [1,4]. BNC is known for its sustainability, biocompatibility, non-toxicity, and high biodegradability. Taken together, the listed properties of this polysaccharide have generated interest in various industries, including biomedicine [2,5,6], pharmaceuticals [7], bioelectronics [3], food industry [8], cosmetics [9], pulp and paper industry [10], and textile industry [11,12]. In recent years, interest in the manufacture of BNC on a large commercial scale has increased significantly [13]. However, the cost of BNC remains high, which limits its widespread use [14]. Currently, many researchers are exploring if carbon and nitrogen sources in the BNC production can be replaced by alternative components in order to increase the yield and reduce the production costs. The nutrient medium must contain carbon and nitrogen required for bacterial growth, and the ratio of these components directly or indirectly affects the BNC formation [15]. Biotechnological approaches have enabled the use of industrial byproducts and lignocellulosic biomass as low-cost and readily available sources of these nutrients, contributing to the economic and energy benefits of the process [16–18]. However, the quality of BNC derived on hydrolyzate nutrient media is a matter of debate. Some authors report that the structure of BNC does not change when one of the components of the nutrient media is replaced or when alternative nutrient media are utilized [19–23], while others have observed such changes [16,24–31]. There are published studies in which some authors deliberately add chemical substances into nutrient media, while the other researchers use various nutrient media, do not analyze their component composition, but discuss the dependence of the BNC quality on the replacement of the nutrient medium [16,24–31]. The replacement of mannitol by sucrose in the nutrient medium led to a decrease in crystallinity from 65.5% to 49.7% [31]. Biosynthesis of BNC by the strain *Komagataeibacter europaeus* KFET1 on an enzymatic hydrolyzate of rice bran showed a decrease in crystallinity to 72% compared to the Hestrin and Schramm (HS) medium (88%) [16]. The crystallinity values of BNC obtained on hydrolyzates of vinegar residue, paper mulberry, and seagrass were 77, 68, and 63%, respectively, which is higher than that on the HS medium (67%) in the first case and lower in the third case [25]. The crystallinity of BNC derived on a hydrolyzate of ramie fibers is 68.05%, which is lower than 82.09% for BNC derived on the HS medium [26].

Natural cellulose can consist of two crystalline allomorphs: Iα cellulose and Iβ cellulose [30,32–34]. Cellulose Iα is basically found in bacterial biofilms and algae, while cellulose Iβ is mainly found in terrestrial plants and tunicates; therefore, BNC is characterized by a Iα-to-Iβ-cellulose ratio that can vary depending on cultivation conditions, such as agitation rather than static conditions, temperature variations or supplement addition [24,30]. The presence of additives interferes with the aggregation of the elementary fibrils into the normal ribbon assembly, and chemically addition media may result in increased contents of Iβ crystal structure [30]. The study [24] described a complex dependence of the cellulose Iβ fraction in BNC (a *G. xylinus* NRRL B-42 microbial producer) upon transition from the HS medium (31% cellulose Iβ fraction) to alternative media, namely: 44% and 42% when switching to commercial glycerol and glycerol from biodiesel, respectively, and 28% and 29% when switching to grape bagasse and cane molasses, respectively. The cellulose Iα content in BNC obtained on hydrolyzates of vinegar residue, paper mulberry, and seagrass was 92%, 88%, and 68%, respectively, which is higher than that on the HS medium (80%) for the first two sources and lower in the third case, respectively [25].

https://doi.org/10.3390/polysaccharides7040124

The literature analysis indicates that a study of the structural features of BNC synthesized on alternative nutrient media is highly relevant. However, the lack of comprehensive published results on this topic makes it difficult to compare experimental data. Despite the growing number of studies on BNC in alternative media, most of them are limited to assessing the yield, degree of crystallinity (DC), and, less frequently, Iα/Iβ allomorph ratio. At the same time, the supramolecular structure of the crystalline component—the unit cell parameters and angles, sizes and shapes of coherent scattering domains (CSD), and anisotropy of crystallites—has not been systematically studied. Full-profile analysis (the Rietveld method) combined with diffractogram recording in two geometries (reflection and transmission) makes it possible to acquire these characteristics with high accuracy and reveal textural effects, which are usually ignored in standard analysis of X-ray diffraction patterns [23–30].

Miscanthus is a perennial rhizomatous grass that has gained recognition as a promising energy crop due to its high biomass yield, low requirements for cultivation conditions, and broad adaptability. In Russia, miscanthus has been cultivated and recommended for planting over the past five years and is grown on farms in the Kaluga, Moscow, Bryansk, Kaliningrad, Penza, Novosibirsk, and Irkutsk regions [35]. This plant was chosen as a substrate for the synthesis of bacterial nanocellulose (BNC) due to its high cellulose content, availability, and potential for use as a renewable non-food feedstock for biotechnological conversion.

For the first time, BNC samples synthesized on miscanthus enzymatic hydrolyzates will be studied by X-ray diffraction analysis to determine the unit cell parameters, degree of crystallinity, and crystallite sizes using a full-profile analysis (the Rietveld method).

The present study aimed to examine the structural features of BNC synthesized by the SCOBY microbial producer on enzymatic hydrolyzates prepared from the energy crop *Miscanthus* × *giganteus*.

2. Materials and Methods

2.1. Materials

Miscanthus × *giganteus* cv. KAMIS (hereinafter referred to as miscanthus) from the Russian breeding stock was grown in the village of Marushkino, the Moscow region, and was provided by OOO "Master Brand" (Moscow, Russia).

2.2. Chemical Pretreatment of Miscanthus × *giganteus*

Miscanthus was subjected to chemical pretreatment at atmospheric pressure under laboratory conditions using four different methods (Table 1), as reported in [36].

Table 1. Summary of BNC samples (1–5), derived on the control medium and on enzymatic hydrolyzate (EH) substrates, pretreatment methods, and hydrolysis conditions.

Sample No.	Substrate Preparation Method	Nutrient Medium	Enzymatic Hydrolysis Conditions	Nutrient Medium Preparation
1	–	Control	–	commercial glucose 20 g/L; black tea extractives 1.6 g/L
2	Single-stage treatment with HNO_3 (substrate 1)	EH substrate 1	initial substrate concentration 3%, stirring rate 150 rpm, temperature (46 ± 2) °C, 0.05 M acetate buffer (pH 4.7)	standardization to a glucose concentration of 20 g/L; black tea extractives 1.6 g/L
3	Single-stage treatment with NaOH (substrate 2)	EH substrate 2		
4	Treatment of substrate 1 with NaOH (substrate 3)	EH substrate 3		
5	Treatment of substrate 2 with HNO_3 (substrate 4)	EH substrate 4		

2.3. Enzymatic Hydrolysis

The resultant chemical treatment products were used as substrates for enzymatic hydrolysis. The hydrolysis conditions were the same for all four types of substrates and are detailed in [36]. Enzymatic hydrolysis was performed using a cocktail of enzymes Agrocell Plus (Agroferment LLC, Novosibirsk, Russia), Cellolux-A (Sibbiofarm LLC, Berdsk, Russia), and Ultraflo Max (Novozymes A/S, Copenhagen, Denmark) (1:1:1). After 72-h hydrolysis, the suspension was vacuum-filtered, and the filtrate was analyzed for reducing sugars (RS), glucose and pentose concentrations. The concentration of RS was quantified on a glucose basis using a 3,5-dinitrosalicylic acid reagent (Panreac, Castellar del Vallès, Spain) [37] on a Cary 60 UV-Vis spectrophotometer (Agilent Technologies, Santa Clara, CA, USA). The glucose concentration was quantified by the glucose oxidase-peroxidase method using reagents from the Fotoglyukosa kit (Impact LLC, Moscow, Russia) [38]. The concentration of pentoses on a xylose basis was quantified spectrophotometrically using an orcin solution [39]. The composition of the prepared hydrolyzates is presented in Table 2.

Table 2. Composition of enzymatic hydrolyzates.

Substrate	* RS Content, g/L	Glucose Content, g/L	Xylose Content, g/L	pH
1	26.90 ± 0.20 ^{c}	24.70 ± 0.20 ^{c}	2.00 ± 0.00 ^{a}	4.90 ± 0.12 ^{a}
2	25.20 ± 0.06 ^{d}	23.00 ± 0.07 ^{d}	1.10 ± 0.06 ^{b}	4.90 ± 0.00 ^{a}
3	28.10 ± 0.15 ^{b}	27.50 ± 0.10 ^{b}	0.50 ± 0.10 ^{d}	4.90 ± 0.06 ^{a}
4	29.30 ± 0.05 ^{a}	28.50 ± 0.20 ^{a}	0.90 ± 0.00 ^{c}	4.90 ± 0.12 ^{a}

* RS, reducing sugars. ANOVA: RS $F(3.8) = 535.7$, $p < 0.0001$; glucose $F(3.8) = 807.7$, $p < 0.0001$; xylose $F(3.8) = 355.1$, $p < 0.0001$; pH $F(3.8) = 0$, $p = 1.000$. Values with the same superscript letters are not significantly different ($p > 0.05$), whereas those with different superscript letters differ significantly ($p < 0.05$).

2.4. Preparation of Nutrient Media

The control medium contained 20 g/L of commercial glucose and 1.6 g/L of black tea extractives. This medium is referred to as the "control" because it does not contain components of lignocellulosic hydrolyzates and serves as a reference for comparison with hydrolyzate media [30,40,41].

Since the enzymatic hydrolysis efficiency differed for the four types of substrates due to different chemical treatment methods used, the obtained hydrolyzates were standardized to a glucose concentration of 20 g/L. The hydrolyzates were filtered, and long-leaf black tea was added at 100 °C at a concentration of 10 g/L. Nutrient media containing black tea extractives at a concentration of 1.6 g/L were thus prepared. The media were filtered to remove residual tea and used for BNC biosynthesis, similarly to the other work [42].

2.5. BNC Biosynthesis and Purification

BNC biosynthesis was carried out under optimal conditions [41]: 27 °C, 9 days, and static cultivation. SCOBY (a microbial consortium of yeast and acetic acid bacteria), which is a consortium traditionally used for the fermentation of kombucha tea, was used as the microbial producer. The species belonging to *Komagataeibacter* (*K. xylinus*, *K. kombuchae*), Acetobacter (*A. aceti*, *A. pasteurianus*, *A. nitrogenifigens*), and *Gluconacetobacter* (*G. sacchari*) are the main AAB strains, whereas *Saccharomyces* strains (*S. cerevisiae*) and non-*Saccharomyces* (*Candida spp.*, *Schizosaccharomyces spp.*, *Dekkera spp.*, *Brettanomyces spp.*) are the leading yeast representatives [43]. SCOBY was purchased from the All-Russian Collection of

Industrial Microorganisms (Pushchino, Moscow Region, Russia). The inoculation dose was 10%.

The BNC samples were purified from nutrient medium residues and cells by sequential treatment with a 2.0% sodium hydroxide solution and a 0.25% dilute hydrochloric acid solution, followed by washing with distilled water [44]. BNC films were freeze-dried in an HR7000-M freeze-drier (Harvest Right LLC, Salt Lake City, UT, USA).

2.6. Sample Preparation for Analysis

For all analytical measurements (FTIR spectroscopy, SEM, and XRD), the BNC samples were used as freeze-dried purified films. The BNC films were dried in a freeze-dryer (Harvest Right LLC, Salt Lake City, UT, USA). The film thickness of the five samples is given in Table 3 and falls within the range of 0.7–1.0 mm. The diameter of the BNC films is 55 mm (Figure 1). For analytical measurements, they were cut into fragments of about 10 × 10 mm in size. No milling, dispersion, or ultrasonic treatment of BNC was applied.

Table 3. BNC biosynthesis parameters after cultivation.

BNC Sample	Cell Count		pH	Concentration, g/L			BNC Film Weight, g	BNC Film Thickness, mm	BNC Yield (on an RS basis), %	Productivity, g/(L·Day)
	Yeast, 10^6 CFU/mL	* AB, 10^6 CFU/mL		** RS	Glucose	Xylose				
1	15 ± 5.0 ^{a}	14 ± 2.0 ^{a}	2.70 ± 0.10 ^{b}	1.10 ± 0.60 ^{e}	1.00 ± 0.15 ^{c}	–	0.1300 ± 0.0053 ^{a}	1.0 ± 0.1 ^{a}	12.00 ± 0.10 ^{a}	0.12 ± 0.01 ^{a}
2	11 ± 3.79 ^{a}	9·10^6 ± 1.53 ^{ab}	3.10 ± 0.15 ^{a}	2.10 ± 0.10 ^{d}	0.60 ± 0.00 ^{d}	1.50 ± 0.10 ^{a}	0.0900 ± 0.0029 ^{b}	0.8 ± 0.1 ^{ab}	8.30 ± 0.00 ^{c}	0.10 ± 0.0 ^{ab}
3	11 ± 1.53 ^{a}	7 ± 1.00 ^{b}	3.30 ± 0.12 ^{a}	7.00 ± 0.06 ^{a}	6.20 ± 0.21 ^{a}	0.60 ± 0.12 ^{b}	0.0800 ± 0.0045 ^{b}	0.7 ± 0.1 ^{b}	7.80 ± 0.10 ^{c}	0.08 ± 0.01 ^{b}
4	18 ± 1.73 ^{a}	13 ± 3.00 ^{a}	3.30 ± 0.20 ^{a}	3.90 ± 0.12 ^{c}	3.60 ± 0.12 ^{b}	0.50 ± 0.00 ^{b}	0.0900 ± 0.0026 ^{b}	0.9 ± 0.1 ^{ab}	10.30 ± 0.20 ^{b}	0.10 ± 0.02 ^{ab}
5	17 ± 1.15 ^{a}	12 ± 2.00 ^{a}	3.30 ± 0.12 ^{a}	4.00 ± 0.10 ^{b}	4,10 ± 0.10 ^{b}	0.80 ± 0.10 ^{ab}	0.1000 ± 0.0031 ^{b}	0.8 ± 0.1 ^{ab}	9.70 ± 0.15 ^{b}	0.10 ± 0.02 ^{ab}

* AB, acetobacteria; ** RS, reducing sugars.; ANOVA: yeast CFU ($F(4.10) = 3.72$, $p = 0.041$), acetic acid bacteria CFU ($F(4.10) = 6.92$, $p = 0.006$), pH ($F(4.10) = 10.61$, $p = 0.001$), reducing substances ($F(4.10) = 1335.4$, $p < 0.0001$), glucose ($F(4.10) = 947.6$, $p < 0.0001$), xylose ($F(3.8) = 103.3$, $p < 0.0001$), film mass ($F(4.10) = 10.68$, $p = 0.001$), film thickness ($F(4.10) = 3.60$, $p = 0.044$), BNC yield ($F(4.10) = 47.60$, $p < 0.0001$), and productivity ($F(4.10) = 5.50$, $p = 0.013$). Values sharing at least one common superscript letter are not significantly different ($p > 0.05$), whereas values with no common superscript letters differ significantly ($p < 0.05$).



Figure 1. BNC samples.

2.7. FTIR Spectroscopy

To acquire information on the molecular structure of the BNC samples, Fourier transform infrared (FTIR) spectroscopy was used. An Infralum FT-801 FTIR spectrometer (NPF Lumex-Sibir LLC, Novosibirsk, Russia) was used with single-pass attenuated total reflectance (ATR) in the frequency range of 4000–600 cm^{-1}.

2.8. SEM Analysis

The morphology of the obtained BNC samples was studied by scanning electron microscopy (SEM).

2.9. XRD Analysis

Diffractograms of the BNC samples were recorded on a DRON-6 diffractometer (Burevestnik JSC, Saint-Petersburg, Russia). CuKα radiation (λ = 1.54178 Å) was monochromatized by a pyrolytic graphite crystal placed in the primary beams. Diffraction patterns were recorded in reflection and transmission geometries in the scattering angle range 2θ from 3° to 145° with steps of 0.1° (from 3° to 50°) in the region of the main Bragg reflections and 0.5° (from 50° to 145°), as recommended in [23,26,27,30,45].

The crystallinity degree (CD) of the studied BNC samples was estimated via Equation (1) as the relation between the integrated scattering intensity from the crystalline phase and the total integrated scattering intensity from the crystalline and amorphous phases:

$$\boldsymbol{CD = \frac{I_c - I_{am}}{Ic} * 100\ \%} \quad (1)$$

where $\boldsymbol{I_c}$ is the total integrated scattering intensity from the crystalline and amorphous phases and $\boldsymbol{I_{am}}$ is the integrated scattering intensity from the amorphous phase. The calculation procedure relies on the Ruland method and is employed in many studies [1,30,32,33,45–50].

The Iα-to-Iβ-cellulose ratio in the samples under study was refined using a full-profile analysis of polycrystalline X-ray diffraction patterns (the Rietveld method) [28,30,32,33,45,46,51]. The data on celluloses Iα and Iβ reported in [51,52] were used as the initial structural characteristics. The reflection profiles were approximated by the pseudo-Voigt function, and the coefficient determining the ratio of the Gaussian and Lorentzian (Cauchy) functions was refined (the methodology is detailed in the Supplementary Materials with Figures S2–S6).

The size of crystalline domains (mosaic blocks, coherent scattering domains (CSDs)) was calculated using the Scherrer equation (Equation (2)) [26,27,29,46,53]:

$$\boldsymbol{\beta_{Scherrer} = \frac{0.94\lambda}{D_{hkl} \cdot cos\theta}} \quad (2)$$

where $\boldsymbol{\beta_{Scherrer}}$ is the line broadening due CSD sizes (integral width of the line, close in magnitude to the width at half height); $\boldsymbol{\lambda}$ is the radiation wavelength; $\boldsymbol{D_{hkl}}$ is the sought-for effective size of the CSD in the direction normal to the reflecting planes with indices $\boldsymbol{hkl}$; $\boldsymbol{\theta}$ is the Bragg angle. Under the Gaussian and Cauchy approximations, the $\boldsymbol{\beta_{Scherrer}}$ values were calculated using the formulas:

$$\boldsymbol{\beta^2_{Scherrer} = B^2 - b^2 \text{ and } \beta_{Scherrer} = B - b, \text{ respectively}} \quad (3)$$

where $\boldsymbol{B}$ and $\boldsymbol{b}$ are the full width at half maximum (FWHM) of the diffraction peaks for the sample and the standard, respectively. The CSD sizes calculated using these two approximations define the range within which the true values lie. For further analysis, the average values were used.

The reliability of the results was assessed by calculating standard R-factors (the unweighted (R_p) and weighted (R_{wp}) profile reliability factors):

$$\boldsymbol{R_p = \frac{\sum_{i=1}^{N}\left[I_i^{exp} - I_i^{theor}\right]}{\sum_{i=1}^{N} I_i^{theor}};\ R_{wp} = \frac{\sum_{i=1}^{N} w_i [I_i^{exp} - I_i^{theor}]^2}{\sum_{i=1}^{N} w_i [I_i^{theor}]^2}} \quad (4)$$

where ($\boldsymbol{I_i^{exp}}$) and ($\boldsymbol{I_i^{theor}}$) are the experimental and calculated intensities at each point of the XRD pattern.

2.10. Statistical Analysis

The experiments were performed in three independent biological replicates. For each sample, three independent BNC films were obtained during the three individual biosynthesis cycles. XRD measurements were performed for each film in reflection and transmission geometries, and the results were averaged over the three independent films.

The experimental results were obtained in triplicate and statistically analyzed by one-way analysis of variance (ANOVA). The results of one-way ANOVA showed statistically significant differences between the groups ($p < 0.05$), followed by a Tukey HSD post hoc test using OriginPro 8.5 (OriginLab Corporation, Northampton, MA, USA). Differences were considered statistically significant at $p < 0.05$. XRD data were analyzed by the Rietveld full-profile refinement method; the uncertainties in the unit cell parameters and the CSD sizes were calculated from the refinement results. The DC values are presented as averages obtained in reflection and transmission geometries, with an uncertainty of ±5%.

3. Results and Discussion

3.1. FTIR Spectroscopy

Table 4 (Figure S1 in the Supplementary Materials) presents the main characteristic absorption band frequencies of functional groups in the BNC samples.

Table 4. Absorption band assignment for functional groups in BC samples.

Absorption Band Assignment *	**Absorption Band Peak, cm^{-1}**				
	1	**2**	**3**	**4**	**5**
ν OH-groups involved in intermolecular and intramolecular H-bonding	3345	3347	3347	3347	3347
ν bonds in CH and CH_2 groups	2894	2894	2895	2894	2894
δ HOH bonds due to tightly bound water present	1649	1630	1630	1630	1630
δ CH_2, CH groups	1427	1427	1427	1427	1427
	1361	1360	1359	1359	1359
δ OH groups in CH_2OH	1335	1335	1335	1335	1335
		1316	1316	1316	1316
ν C-O bonds (bands typical of polysaccharides due to present C-O-C acetyl bonds and C-O bonds in alcohols)	1161	1161	1161	1161	1160
	1055	1056	1057	1057	1057
	1032	1033	1034	1034	1034
β-1,4 linkages	899	898	899	898	898

* ν, stretching; δ, bending.

The broad band near 3345–3347 cm^{-1} corresponds to O–H stretching vibrations, indicating the tendency of the materials toward hydrophilicity. The peaks at 294 cm^{-1} correspond to the C–H and CH_2 stretching vibrations, and the vibrations near 1630–1649 cm^{-1} are attributed to the bending vibration of absorbed water molecules [54]. The peaks at 1427 cm^{-1} and near 1359–1361 cm^{-1} are characterized by bending vibrations of the CH_2 and CH groups [55]. Weak absorption bands at 1335 cm^{-1} and 1316 cm^{-1} characterize the bending vibrations of O–H groups. The bands located near 1160–1161 cm^{-1}, 1056–1057 cm^{-1}, and 1032–1034 cm^{-1} are associated with the asymmetric stretching of the C–O–C bridge of the β-glycosidic bond, stretching of the pyranose ring skeleton C–O, and stretching of C–O bonds of the cellulose molecule [54]. The band near 898–899 cm^{-1} corresponds to the first carbon atom involved in the formation of the β-glycosidic bond [55].

Based on the presented FTIR spectroscopy data, it was shown that, regardless of the nutrient medium composition, all BNC samples were identical and represented pure cellulose. The spectral characteristics are consistent with the published data [54,55].

3.2. SEM Analysis

SEM images are depicted in Figure 2.

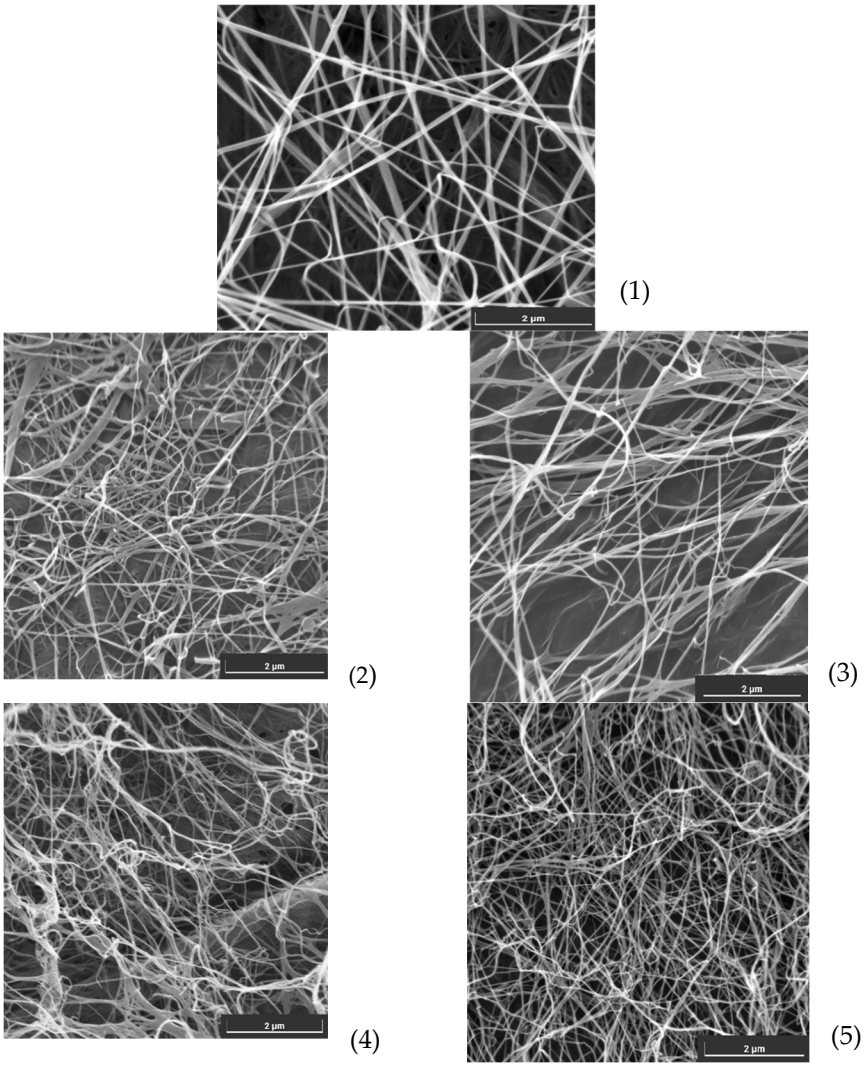


Figure 2. SEM micrographs of BNC samples: (**1**) BNC 1 (control), (**2**) BNC 2 (EH substrate 1), (**3**) BNC 3 (EH substrate 2), (**4**) BNC 4 (EH substrate 3), and (**5**) BNC 5 (EH substrate 4); ×30,000 magnification.

The SEM examination showed that the obtained BNC samples synthesized on the control nutrient medium and on the media prepared from miscanthus enzymatic hydrolyzates have a reticulate structure representing a nanofiber network, which is typical of BNC [25,28]. For further study of the morphological characteristics, 100 BNC fibers were randomly selected and their diameter distributions and mean diameters were calculated manually from the SEM patterns. The average width of BNC nanofibers was 52 nm for the sample obtained on the control medium; 47 nm for the sample obtained on the nutrient medium of enzymatic hydrolyzate of substrate 1; 53 nm for the sample obtained on the nutrient medium of enzymatic hydrolyzate of substrate 2; 52 nm for the sample obtained on the nutrient medium of enzymatic hydrolyzate of substrate 3; and 38 nm for the sample obtained on the nutrient medium of enzymatic hydrolyzate of substrate 4. The data

obtained are comparable to the literature data; for example, the average fiber width is 35 nm for BNC obtained from a seagrass medium, 60 nm for BNC obtained from vinegar residue, and 58 nm for BNC obtained from paper mulberry [25].

3.3. XRD Analysis

Figure 3 shows fragments of the scattering intensity distribution curves of the studied BNC samples, recorded in reflection and transmission geometries, as compared with the theoretical X-ray pattern of cellulose Iα calculated in the Free Mercury software [56] using the unit cell periods and angles, and atomic coordinates reported in [32,33,51,52,57].

A group of well-defined Bragg lines is observed within this range of scattering angles; beyond the scattering angle 2θCu ≈ 50°, the lines on the diffractograms overlap and blur to such an extent that they practically merge with the background.

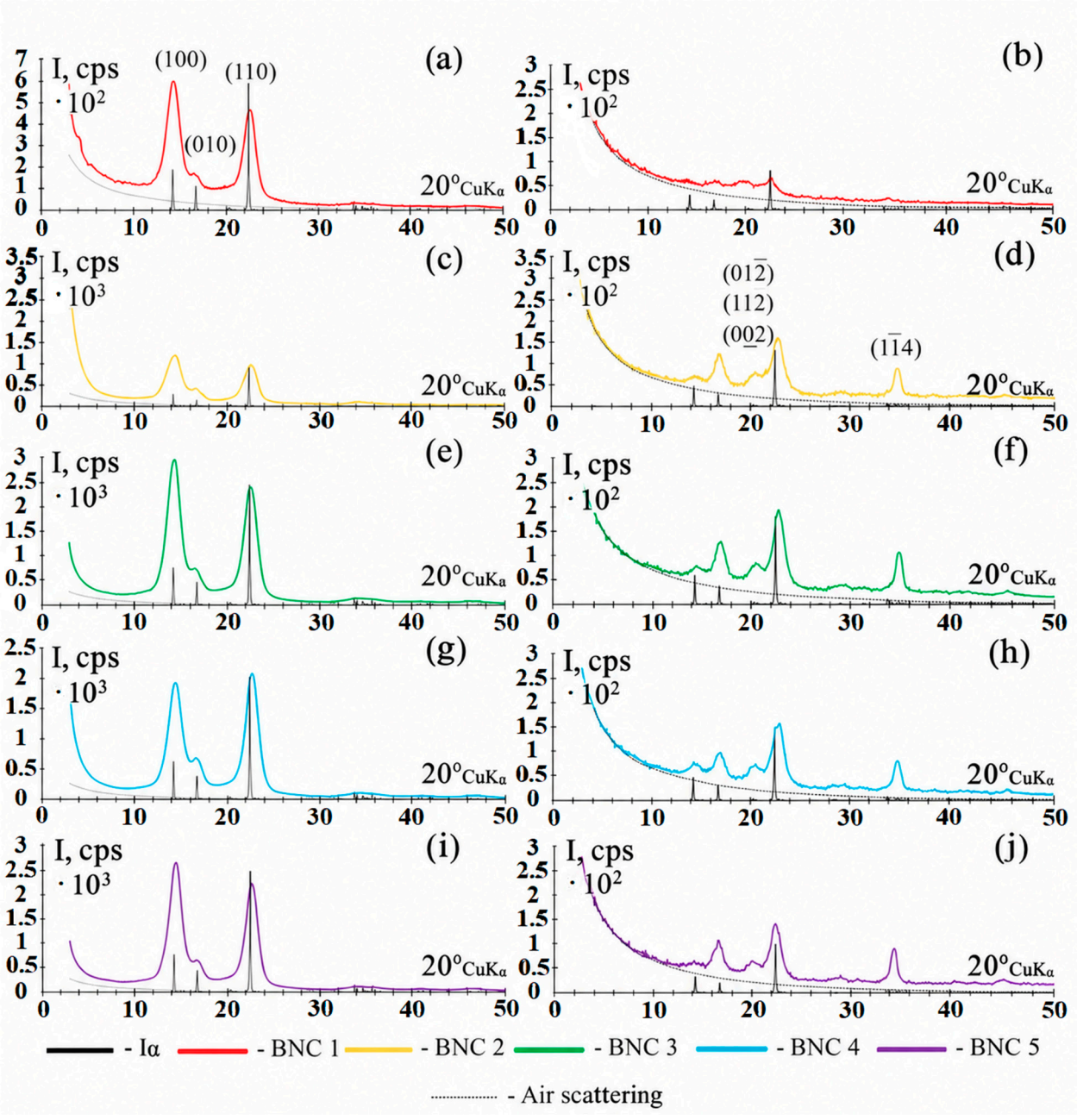


Figure 3. The 2θCu range of diffractograms of BNC samples 1–5 from 3° to 50° recorded in (**a**,**c**,**e**,**g**,**i**) reflection and (**b**,**d**,**f**,**h**,**j**) transmission; the reflection indices are indicated for cellulose Iα allomorph.

It can be seen in Figure 3 that the experimental X-ray diffraction images recorded in two geometries for BNC samples 1–5 align in reflection positions with the theoretical curve constructed for the cellulose Iα model. The observed redistribution of intensities on the experimental curves is related to the presence of texture in the thin-film BNC samples.

The diffraction patterns of BNCs derived on different nutrient media show three peaks at 2θ = 14.5° (100), 16.3° (010) and 22.5° (110), confirming that all BNC samples are cellulose I [20,30]. The peak intensity at 2θ 14.5° on the diffraction patterns is higher than that at 2θ 16.3°, indicating that the BNC samples chiefly contain cellulose Iα [58]. Cellulose I represents a crystalline structure with the highest axial elastic modulus [30]. Comparison of the presented data with the results of the studies [16,19,20,26,29,55,59] shows coincidence of the intense reflections. This confirms that the experimental BNC samples correspond not only to cellulose I type, but also to the published data on BNC.

The difference in intensity distribution on the experimental scattering curves obtained in the reflection (Figure 3a,c,e,g,i) and transmission (Figure 3b,d,f,h,j) geometries indicates an anisotropic structure of the experimental BNC samples: the intensity of the main maxima (100) and (010) sharply decreases on the diffraction patterns recorded in transmission, the intensity of the $[11\bar{4}]$ line increases, and a maximum corresponding to the $(01\bar{2})$, $(11\bar{2})$ (002) reflections appears.

It was established in the calculations that the structure of all experimental BNC samples corresponds to cellulose Iα. The full-profile analysis results are outlined in Table 5.

Table 5. Full-profile analysis results: unit cell periods and angles.

Sample No.	1	2	3	4	5
Iα, %	99.2	95.3	96.5	95.4	99.9
Iβ, %	0.8	4.7	3.5	4.6	0.1
a, Å	6.6335(6)	6.6351(3)	6.6522(9)	6.6570(6)	6.63528(4)
b, Å	5.9513(5)	5.9253(8)	5.9426(1)	5.9590(9)	5.9203(7)
c, Å	10.3649(7)	10.3213(1)	10.2922(1)	10.3403(8)	10.3013(1)
α, °	118.2(9)	118.8 (2)	118.1(3)	117.9(3)	118.8 (6)
β, °	111.1(5)	111.4 (5)	112.8 (6)	111.8(6)	111.3(2)
γ, °	82.6(7)	82.2 (3)	82.3(2)	81.6(0)	82.2(1)
V, Å^3	337.2(6)	335.4(8)	335.8(3)	336.1(6)	335.4(4)
T_{100}	2.854	2.968	4.543	3.613	2.336
R_p,%	5.56	6.65	7.83	6.93	7.67
R_{wp},%	9.53	9.57	11.24	9.88	10.86
GofF	0.43	0.74	0.72	0.61	0.65

T_{100} is the axial texture parameter with the {100} axis; R_P and R_{WP} are the reliability factors, and GofF is the goodness-of-fit factor for the experimental and calculated diffraction patterns.

The theoretical X-ray pattern corresponds to the cellulose Iα model proposed in [60,61]. The cellulose Iα crystallizes in a triclinic unit cell with parameters *a* = 6.717(7) Å, *b* = 5.962(6) Å, *c* = 10.400(6) Å, α = 118.08(5)°, β = 114.80(5)°, and γ = 80.37(5)°, having space group P1 [60,61]. The similarity of the obtained values in Table 1 to the literature data indicates that the structure of the BNC samples represents cellulose Iα, regardless of the nutrient medium composition, in agreement with the other study [61]. The GofF values below unity are mainly due to the fact that the background region significantly exceeds the region in which Bragg reflections are observed (Figure 3).

The BNC diffractograms are characterized by significant overlap of diffraction maxima, anisotropy, reflection broadening, the influence of preferred crystallite orientation, and the presence of an amorphous component. These features significantly complicate the

quantitative differentiation of structurally similar cellulose Iα and cellulose Iβ polymorphs by the Rietveld method, especially at a low content of either phase.

In the full-profile analysis, the Iα cellulose content in the obtained BNC samples was calculated to be 95–100%. These data are interesting and rather rare. A change in the conventional nutrient medium for BNC biosynthesis can often lead to a decrease in the cellulose Iα fraction. Molasses and vinasse used as carbon sources in the nutrient medium for BNC biosynthesis lead to a decrease in the cellulose Iα content to 63% and 61%, respectively, versus 86% for the HS medium [24].

Figure 4 depicts the experimental scattering curve obtained in reflection geometry for the BNC samples, which was approximated by the total integral intensities.

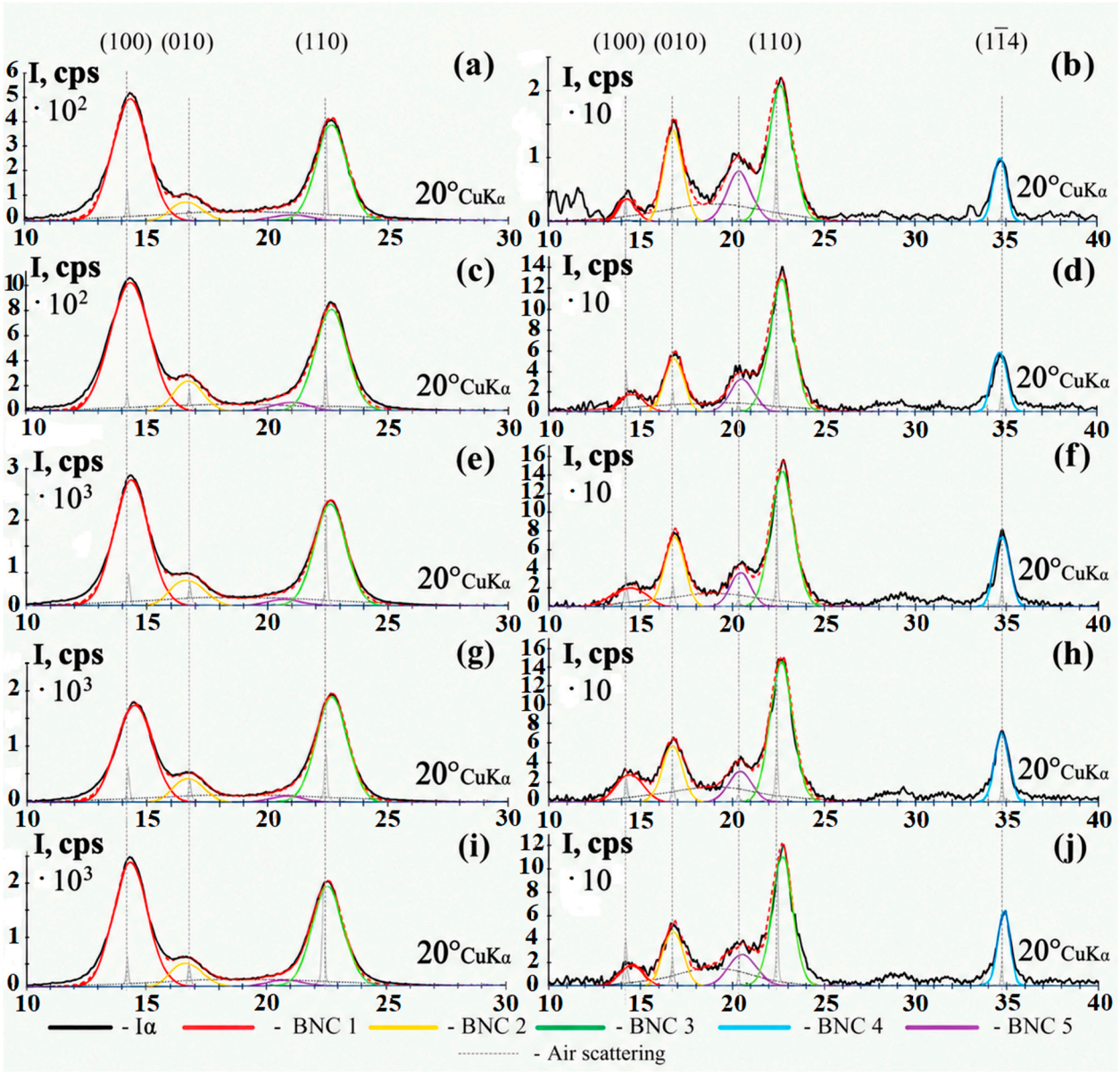


Figure 4. Decomposition patterns of spectra of the celluloses under study into the total integral intensities of all maxima ((**a**,**c**,**e**,**g**,**i**) in reflection geometry and (**b**,**d**,**f**,**h**,**j**) in transmission geometry): — experiment; — — resultant approximating curve; — — amorphous maximum; — (100); — (010); — (01$\bar{2}$) (11$\bar{2}$) (002); — (110); — (11$\bar{4}$) compared with the theoretical X-ray pattern of cellulose Iα (—).

The crystallite size values were obtained from Figure 4 in the [100], [110], and [010] directions (these directions are perpendicular to the fibril axis). These directions

determine the linear dimensions and shape of the cross-section of the elementary fibrils of the cellulose Iα crystal lattice. The obtained CD values, averaged over reflection and transmission, and the mean CSD sizes (Gaussian–Cauchy) are presented in Table 6.

Table 6. CD values averaged over reflection and transmission, and mean CSD sizes (Gaussian–Cauchy) (*hkl*, reflection indices in the X-ray image corresponding to cellulose Iα).

Sample No.	**1**		**2**		**3**		**4**		**5**	
Geometry	R	T	R	T	R	T	R	T	R	T
CD ± 5%	78 ± 2 ^{b}		85 ± 1 ^{a}		83 ± 1 ^{a}		82 ± 1 ^{a}		84 ± 2 ^{a}	
hkl	D_{hkl}^{g-k} ± 0.5 nm									
(100)	5.2 ± 0.3 ^{a}	7.6 ± 0.3 ^{a}	4.4 ± 0.3 ^{b}	6.2 ± 0.3 ^{c}	5.2 ± 0.2 ^{a}	4.0 ± 0.2 ^{d}	4.8 ± 0.2 ^{ab}	5.2 ± 0.2 ^{b}	5.2 ± 0.1 ^{a}	7.6 ± 0.1 ^{a}
(010)	6.2 ± 0.4 ^{a}	7.6 ± 0.4 ^{a}	6.8 ± 0.3 ^{a}	7.6 ± 0.3 ^{a}	5.5 ± 0.3 ^{b}	7.6 ± 0.3 ^{a}	6.2 ± 0.2 ^{a}	7.6 ± 0.2 ^{a}	5.7 ± 0.1 ^{ab}	7.6 ± 0.1 ^{a}
$(01\bar{2})$, $(11\bar{2})$, (002)	4.5 ± 0.1 ^{b}	5.7 ± 0.1 ^{b}	4.5 ± 0.3 ^{b}	5.7 ± 0.3 ^{b}	7.7 ± 0.2 ^{a}	7.7 ± 0.2 ^{a}	7.7 ± 0.2 ^{a}	6.2 ± 0.2 ^{b}	4.9 ± 0.1 ^{b}	4.5 ± 0.1 ^{c}
(110)	6.0 ± 0.3 ^{a}	5.7 ± 0.3 ^{c}	5.7 ± 0.2 ^{a}	5.7 ± 0.2 ^{c}	5.7 ± 0.2 ^{a}	6.3 ± 0.2 ^{b}	5.7 ± 0.1 ^{a}	6.3 ± 0.1 ^{b}	5.7 ± 0.1 ^{a}	6.9 ± 0.1 ^{a}
$(11\bar{4})$	–	12.1 ± 0.5 ^{c}	–	13.0 ± 0.4 ^{bc}	–	14.9 ± 0.4 ^{b}	-	13.6 ± 0.4 ^{bc}	-	18.1 ± 0.4 ^{a}

Data are presented as mean ± SD. R, reflection; T, transmission. Values sharing at least one common superscript letter are not significantly different ($p > 0.05$), whereas values with no common superscript letters differ significantly ($p < 0.05$).

The CSD size in the direction of the elementary fibril length was calculated from the crystallite size in the $[11\bar{4}]$ direction of cellulose Iα, which coincides with the fibril axis. The CSD size values of the BNC samples derived on the control nutrient medium were 5.2 nm in reflection and 7.6 nm in transmission in the [100] direction; 6.2 nm in reflection and 7.6 nm in transmission in the [010] direction; 4.5 nm in reflection and 5.7 nm in transmission in the $[01\bar{2}]$, $[11\bar{2}]$, [002] direction; and 6.0 nm in reflection and 5.7 nm in transmission in the [110] direction. The CSD size values of the BNC samples produced on the nutrient media prepared from enzymatic hydrolyzates were 4.4–5.2 nm in reflection and 4.0–7.6 nm in transmission in the [100] direction; 5.5–6.8 nm in reflection and 7.6 nm in transmission in the [010] direction; 4.5–7.7 nm in reflection and 4.5–7.7 nm in transmission in the $[01\bar{2}][11\bar{2}]$[002] direction; and 5.7 nm in reflection and 5.7–6.9 nm in transmission in the [110] direction. The CSD sizes also differed significantly among the samples in most crystallographic directions (Table 6). In the (100) direction, the CSD size in reflection geometry was significantly larger for sample 1 (5.2 ± 0.3 nm) than for sample 2 (4.4 ± 0.3 nm, $p = 0.038$), while in transmission geometry, sample 1 (7.6 ± 0.3 nm) and sample 5 (7.6 ± 0.1 nm) showed significantly larger CSD sizes than samples 2 (6.2 ± 0.3 nm, $p = 0.003$), 4 (5.2 ± 0.2 nm, $p < 0.0001$), and 3 (4.0 ± 0.2 nm, $p < 0.0001$). In the $[11\bar{4}]$ direction, the CSD size increased in the order of sample 1 (12.1 ± 0.5 nm) < sample 2 (13.0 ± 0.4 nm) ≈ sample 4 (13.6 ± 0.4 nm) < sample 3 (14.9 ± 0.4 nm) < sample 5 (18.1 ± 0.4 nm), with sample 5 being significantly larger than all other samples ($p < 0.01$).

The order of the obtained values is comparable with the data presented in some studies of BNC synthesized on both a control nutrient medium (4.4 nm in the [100] direction, 5.6 nm in the [010] direction, and 5.0 nm in the [110] direction) [29] and a cheese whey medium (6.7 nm in the [002] direction) [28]. The CSD sizes in reflection geometry for BNC samples obtained on different carbon sources range from 4.2 nm to 5.2 nm in the [100] direction, from 5.8 nm to 7.0 nm in the [010] direction, from 5.6 nm to 6.2 nm in the [110] direction, and from 4.4 nm to 5.3 nm [62] in the $(01\bar{2})$ direction, which are generally comparable with the CSD data presented in Table 6. The CSD sizes of BNC obtained on a ramie fiber hydrolyzate are similar (5.6 and 6.2 nm in the [100] and [110] directions, respectively) to the data provided in Table 6; however, they are larger in the [010] direction (9.2 nm) [26]. The CSD values outlined in Table 6 are lower than those for BNC obtained

on media containing Sweet Potato Waste and, specifically, are 9.4 nm in the [010] direction and 7.8 nm in the [110] direction [29]; 20.4 nm in the [110] direction for BNC on a distiller's grain enzymatic hydrolyzate medium [58]; 12.4 nm in the [110] direction for BNC on a whole pineapple peel extract medium; 9.1 nm in the [110] direction for BNC on a whole banana extract medium; and 11.9 nm in the [110] direction for BNC on a mixed pineapple peel and banana extracts medium [54]. The CSD size calculated from the diffraction peak [$11\bar{4}$], corresponding to the crystallite size along the longitudinal direction of BNC elementary fibrils, is lower (7.5–8.7 nm) [62] than those for the BNC samples synthesized on five different nutrient media, as presented in Table 6 (12.1–18.1 nm). For clarity, the results obtained in the present study are presented and compared with published data in Table 7.

Table 7. CSD sizes and DC of BNC samples versus published data.

BNC Sample	Microbial Producer	Nutrient Medium	CSD Sizes, nm					DC, %	Ref.
			R				T		
			(100)	(010)	(01$\bar{2}$) (11$\bar{2}$) (002)	(110)	(11$\bar{4}$)		
1	SCOBY	Control	5.2	6.2	4.5	6.0	12.1	78	Present study
2	SCOBY	EH sub.1	4.4	6.8	4.5	5.7	13.0	85	Present study
3	SCOBY	EH sub.2	5.2	5.5	7.7	5.7	14.9	83	Present study
4	SCOBY	EH sub.3	4.8	6.2	7.7	5.7	13.6	82	Present study
5	SCOBY	EH sub.4	5.2	5.7	4.9	5.7	18.1	84	Present study
K. sucrofermentans DSM 15973		HS medium	–	–	–	–	–	85	[22]
		orange pomace hydrolysate	–	–	–	–	–	93	
K. xylinus DSM 2325		HS medium	–	–	–	–	–	85	[24]
		molasses	–	–	–	–	–	57	
		vinasse	–	–	–	–	–	66	
Kombucha		HS medium	–	–	–	–	–	67	[25]
		vinegar residue	–	–	–	–	–	77	
Novacetimonas hansenii HX1		ramie textile waste	5.6	9.2	–	6.2	–	–	[26]
K.xylinus ATCC 53524		HS medium	–	–	–	–	–	76	[27]
		wheat straw hydrolyzate	–	–	–	–	–	66	
G. xylinus (PTCC 1734)		HS medium	–	–	7.5	–	–	79	[28]
		cheese whey	–	–	6.7	–	–	62	
SCOBY		control	4.4	5.6	–	5.0	–	65	[29]
		sweet potato	7.0	9.4	-	7.8		27	
K. intermedius MO		HS medium	–	–	–	–	–	49.7	[53]
		cheese whey	–	–	–	–	–	25–34	
G. xylinus G29		distiller's grain enzymatic hydrolysate	–	–	–	20.4	–	85.8	[58]
K. hansenii (ATCC 53582)		Different sources of carbon	4.2–5.2	5.8–7.0	4.4–5.3	5.6–6.2	12.1–18.1	82–71	[55]
G. xylinus BNKC 19		whole pineapple peel extract	–	–	–	12.4	–	–	[62]
		whole banana extract	–	–	–	9.1	–	–	
		mixed pineapple peel and banana extracts	–	–	–	11.9	–	–	
K. xylinus ATCC 700178		HS medium	–	–	–	–	–	61	[59]
		waste fig medium	–	–	–	–	–	70	

G., Gluconacetobacter; K., Komagataeibacter; EH, enzymatic hydrolysis; sub., substrate.

CD is commonly used to measure the relative amount of the crystalline fraction of cellulosic materials and quantitatively assess their modification after various

physicochemical and biological treatments [45]. As for the study of BNC, CD is an important quality attribute of polysaccharide, since cellulose crystallinity is known to determine strength, thermal stability, and, consequently, application areas. The crystallinity degree of BNC sample 1 (control medium) was 78%, while that of BNC samples 2–5 (on miscanthus hydrolyzates) was 85%, 83%, 82%, and 84%, respectively. The CD values are averages obtained from reflection and transmission measurements for each BNC sample. The mean CD of BNC samples 2–5 was 83.5%, which is higher than 78% for BNC sample 1.

One-way analysis of variance (ANOVA) revealed statistically significant differences between the groups ($F(4.10) = 18.5$; $p < 0.001$). The Tukey post hoc test showed that the CD value for samples 2–5 was significantly higher than that for sample 1 ($p < 0.001$ for all pairwise comparisons), whereas no statistically significant differences were found between samples 2–5 ($p > 0.05$). The mean CD value for samples 2–5 was 83.5 ± 1%, which is significantly higher than that for sample 1.

The obtained results are higher than those reported in the literature; for example, the CD is 76% for BNC synthesized on an HS medium [23] and 66% for BNC synthesized on a wheat straw hydrolyzate [26] (Table 7). The total replacement of the carbon source (glucose) and the nitrogen source (yeast) with cheese whey contributed to a decrease in the DC of BNC from 49.7% to 25.3% and 33.8%, respectively [53]. The use of molasses as a carbon source and vinasse as a nitrogen source led to a decrease in the CD from 85% (HS medium) to 57% and 66%, respectively [24]. BNC synthesized on an HS medium had a CD of 79% compared with 62% for BNC on cheese whey [28]. The microstructural study of BNC obtained on a medium containing sweet potato waste showed a decrease in CD from 65% to 27% compared with BNC obtained on a control medium containing sucrose and peptone [29]. However, there are also opposite examples in which the DC of BNC obtained on alternative nutrient media is higher than that of BNC obtained on the control medium (Table 7). For example, when a waste fig medium was used for biosynthesis, the crystallinity of the BNC sample was 70% compared with 61% for the BNC sample obtained on HS [59]. The use of an orange pomace hydrolyzate as a nutrient medium also contributes to an increase in the CD of BNC to 93% compared with 85% in the case of the HS medium [22]. The CD of the BNC sample synthesized on a nutrient medium from vinegar residue was 77% compared with 67% in the case of HS [25]. The results presented above suggest a complex dependence of the CD of BNC on the alternative nutrient medium compared with the control (Table 7); however, in our work, the CD was observed to increase when the control medium was replaced by four variants of hydrolyzates from chemically treated miscanthus. This may be related to the presence in the hydrolyzates of many minor components (such as organic acids, trace elements, etc.) that can affect the metabolic rate and fiber assembly, thereby altering the final structure of crystallites. The suggested mechanism is that the BNC production rate is inversely correlated with the crystallinity degree [63]. The composition of the nutrient medium affects the metabolic rate of bacteria: due to the more complex and diverse composition of nutrients, the BNC production rate in hydrolyzates may differ from that on a synthetic medium (for instance, the initial production rate may be slower), which gives the cellulose fibrils more time for ordered packing, thereby increasing the CD.

The difference in CSD size values obtained in different geometries for all studied BNC samples indicates anisotropy of the crystallites. The weakest anisotropy is observed for crystallites in the [110] direction, according to the data presented in Table 8: the ratio is close to 1 for BNC samples nos. 1–4 and somewhat higher (1.2) for BNC sample no. 5. Ratios close to the aforesaid data in the [010] direction are observed for BNC samples nos. 1, 2, and 4. For BNC samples nos. 3 and 5, this ratio is close to ~1.4. Similar ratio values are observed for crystallites with the [100] orientation for BNC samples nos. 1, 2, and 5.

The obtained data are similar to those reported in [53], in which the production of bacterial cellulose from isolated and protein waste is described.

Table 8. Ratio of CSD sizes calculated from diffractograms recorded in transmission and reflection geometries.

Sample No.		1	2	3	4	5
[*hkl*] α	(*hkl*) α	T/R ratio (D_{hkl}, nm, Gauss–Cauchy) ±0.05				
100	100	1.46	1.40	0.76	1.08	1.46
010	010	1.23	1.12	1.40	1.23	1.35
110	110	0.95	1.00	1.10	1.10	1.20

T/R, transmission/reflection.

It should be noted that the linear crystallite size in a direction can only be determined from the width of the $[11\bar{4}]$ reflection observed on the diffractogram recorded in transmission (Table 6). The maximum crystallite size in this direction is found in BNC sample no. 5 (18.1 nm), while the minimum in BNC sample no. 1 (12.1 nm). The anisotropy of the crystallites is provided in more detail in the Supplementary Materials.

For the first time, a comprehensive X-ray diffraction analysis of BNC samples synthesized on enzymatic hydrolyzates of pretreated miscanthus (*Miscanthus* × *giganteus* cv. KAMIS) using the SCOBY producer was carried out in comparison with a control medium. The comparison with the results published in our previous study [64], which reported an X-ray diffraction analysis of BNC samples obtained on enzymatic hydrolyzates of another miscanthus (*Miscanthus sacchariflorus* Maxim.), showed that the unit cell parameters of BNC in both works are close to each other and correspond to Iα cellulose. Also, the results obtained in the reflection and transmission geometries revealed the anisotropy of crystallites. However, in the present work, the anisotropy was quantitatively characterized through the T/R ratio, which is a more detailed analysis compared with [64]. Unlike [64], this study specifies the Iα cellulose content, namely: all BNC samples fall within the range of 95–100%. In [64], the crystallinity values of BNC were in the range of 86–94%, and there was no control. In the present work, the degree of crystallinity of BNC prepared on hydrolyzates was determined by more accurate calculations using the Rietveld method and has a higher value (82–85%) compared with the control medium (78%). The CSD sizes in the [100], [010], and [110] directions are somewhat smaller (4.0–7.6 nm) in the present work than 4.7–10.8 nm reported in [64]. However, the longitudinal CSD size in the $[11\bar{4}]$ direction is larger (12.1–18.1 nm versus 9.4–16.1 nm) in the present work and may indicate more elongated crystallites. Overall, this study represents a more detailed examination of experimental BNC samples by X-ray diffraction analysis versus the control.

A full comparison of the obtained results on the CSD sizes and DC of the experimental BNC samples with the published data presented in Table 7 allows for the conclusion that the high structural characteristics of the obtained BNC samples are due to the use of the SCOBY producer, since the symbiotic consortium is distinguished by a high adaptive potential and ensures the cultivation of BNC with a stable structure, regardless of the nutrient medium composition.

4. Conclusions

In this work, for the first time, BNC samples synthesized using the symbiotic culture SCOBY on enzymatic hydrolyzates prepared from chemically treated *Miscanthus* × *giganteus* (cv. KAMIS) and on a control glucose medium were studied by X-ray diffraction analysis. X-ray diffraction analysis was performed in two geometries (reflection and

transmission) using a full-profile analysis (the Rietveld method), and structural characteristics such as unit cell parameters and angles, crystallinity degree (CD), coherent scattering domain (CSD) sizes, and crystallite anisotropy were determined.

The following key results were established:

- All five BNC samples, regardless of the nutrient medium composition, were identified as Iα cellulose. The unit cell parameters and angles of all five samples are identical within the experimental uncertainty. The Iα cellulose content in the five BNC samples was 95–100%.
- The CSD sizes in the directions perpendicular to the fibril axis ([100], [010], [110]) for all samples were 4.0–7.7 nm. The CSD size along the fibril axis (direction [11$\bar{4}$]) varied from 12.1 nm (sample 1) to 18.1 nm (sample 5). This indicates that the hydrolyzate composition affects the longitudinal growth of crystallites to a greater extent rather than their transverse dimensions.
- The BNC samples obtained on enzymatic hydrolyzates demonstrated a higher degree of crystallinity (85, 83, 82 and 84%) compared with the sample synthesized on the control medium (78%). This indicates that replacing the synthetic medium with miscanthus hydrolyzates improves the BNC quality.
- The crystallites of all the studied BNC samples are anisotropic, which is confirmed by the difference in the CSD sizes obtained in the reflection and transmission geometries. The T/R ratio varied from 0.76 to 1.46, depending on the crystallographic direction and the sample.
- The composition of the media derived from miscanthus hydrolyzates (prepared by four different chemical pretreatments) had no significant effect on the Iα cellulose content, crystallite sizes, or DC of BNC. This indicates the high stability of the SCOBY consortium as the microbial producer that ensures the reproducibility of the structural characteristics of BNC, regardless of the nutrient medium composition, which is especially important for the development of cost-effective BNC production on alternative media.

Supplementary Materials: The following supporting information can be downloaded at: https://www.mdpi.com/article/10.3390/polysaccharides7040124/s1, Figures S1–S7 showing IR spectra and structural parameters refinement of BNC samples; X-ray diffraction description.

Author Contributions: Conceptualization, E.K.G.; methodology O.V.T. and L.A.A.; software, O.V.T. and L.A.A.; validation, V.V.B.; formal analysis, E.K.G.; investigation, A.A.Z., E.K.G. and E.I.K.; visualization, O.V.T. and L.A.A.; data curation, E.A.S.; writing—original draft preparation, E.K.G. and V.V.B.; writing—review and editing, E.K.G. and V.V.B.; supervision, E.K.G. and V.V.B. All authors have read and agreed to the published version of the manuscript.

Funding: The research was carried out at the expense of the Russian Science Foundation grant No. 22-13-00107-P, https://rscf.ru/project/22-13-00107/ (accessed on 10 June 2025).

Institutional Review Board Statement: Not applicable.

Data Availability Statement: Data is contained within the article or Supplementary Materials.

Acknowledgments: This work was carried out using equipment provided by the Biysk Regional Center for Shared Use of Scientific Equipment of the SB RAS (IPCET SB RAS, Biysk, Russia).

Conflicts of Interest: The authors declare no conflicts of interest.

References

1. Efremenko, E.; Aslanli, A.; Stepanov, N.; Senko, O.; Chumachenko, I.; Domnin, M. Biosynthetic Composites Based on Bacterial Cellulose and Synthetic Polymers: In Silico Prediction of Combinations and In Situ Characterization. *Polysaccharides* **2026**, *7*, 86. https://doi.org/10.3390/polysaccharides7030086.
2. Bulkina, A.; Prilepskii, A. Bacterial cellulose: Is it really a promising biomedical material? *Carbohydr. Polym.* **2025**, *357*, 123427. https://doi.org/10.1016/j.carbpol.2025.123427.
3. Hu, S.; Shi, Z.; Chen, K.; Chen, X.; Zhou, H.; Yan, N.; Yang, G. Bacterial cellulose as green matrix material for environmental-friendly electronic devices. *Carbohydr. Polym.* **2025**, *368*, 124075. https://doi.org/10.1016/j.carbpol.2025.124075.
4. Tran, G.T.; Nguyen, T.T.T.; Nguyen, D.T.C.; Tran, T.V. Bacterial cellulose and composites for the treatment of water pollution: A review. *Environ. Chem. Lett.* **2025**, *23*, 707–732. https://doi.org/10.1007/s10311-025-01818-7.
5. Loya-Hernández, L.P.; Arzate-Quintana, C.; Castillo-González, A.R.; Camarillo-Cisneros, J.; Romo-Sáenz, C.I.; Favila-Pérez, M.A.; Quiñonez-Flores, C.M. Propolis-Functionalized Biomaterials for Wound Healing: A Systematic Review with Emphasis on Polysaccharide-Based Platforms. *Polysaccharides* **2025**, *6*, 74. https://doi.org/10.3390/polysaccharides6030074.
6. Soares, A.L.d.B.; Luz, E.P.C.G.; Castro-Silva, I.I.; Monteiro, R.R.d.C.; Andrade, F.K.; Vieira, R.S. Composite Based on Biomineralized Oxidized Bacterial Cellulose with Strontium Apatite for Bone Regeneration. *Polysaccharides* **2025**, *6*, 23. https://doi.org/10.3390/polysaccharides6010023.
7. Campano, C.; Rivero-Buceta, V.; Hernandez-Arriaga, A.M.; Manoli, M.T.; Prieto, M.A. Pushing the limits of bacterial cellulose for biomedicine: A review. *Int. J. Biol. Macromol.* **2025**, *323*, 146701. https://doi.org/10.1016/j.ijbiomac.2025.146701.
8. Wang, Z.; Li, S.; Zhao, X.; Liu, Z.; Shi, R.; Hao, M. Applications of bacterial cellulose in the food industry and its health-promoting potential. *Food Chem.* **2025**, *464*, 141763. https://doi.org/10.1016/j.foodchem.2024.141763.
9. Kumaravel, A.; Lin, S.P.; Santoso, S.P.; Shanmugasundaram, S.; Hsu, H.Y.; Hsieh, C.W.; Chou, Y.-C., Lin, H.-W., Cheng, K.C. Unlocking the potential of bacterial cellulose: Synthesis, functionalization, and industrial impact. *Int. J. Biol. Macromol.* **2025**, *311*, 143951. https://doi.org/10.1016/j.ijbiomac.2025.143951.
10. Quijano, L.; Rodrigues, R.; Fischer, D.; Tovar-Castro, J.D.; Payne, A.; Navone, L.; Hu, Y.; Yan, H.; Pinmanee, P.; Poon, E.; Yang, J.; Barro, E. Bacterial cellulose cookbook: A systematic review on sustainable and cost-effective substrates. *J. Bioresour. Bioprod.* **2024**, *9*, 379–409. https://doi.org/10.1016/j.jobab.2024.05.003.
11. Zhu, S.; Sha, Y.; Shan, J.; Chen, T.; Yang, J.; Peng, H.; Zhang, R.; Chen, Y.; Sun, W. Bacterial cellulose: A sustainable material for environmental applications. *Cellulose* **2026**, *33*, 607–630. https://doi.org/10.1007/s10570-025-06905-0.
12. Fernandes, M.; Souto, A.P.; Dourado, F.; Gama, M. Application of Bacterial Cellulose in the Textile and Shoe Industry: Development of Biocomposites. *Polysaccharides* **2021**, *2*, 566–581. https://doi.org/10.3390/polysaccharides2030034.
13. Mukherjee, P.; Kamble, R.D.; Krishnan, J.B.; Sivaprakasam, S.; Sekharan, S. Bacterial cellulose production, scale-up, and applications: A techno-economic study of industry-ready bacterial cellulose production from industrial and agro wastes. *Cellulose* **2025**, *33*, 541–570. https://doi.org/10.1007/s10570-025-06896-y.
14. Mikaeeli Kangarshahi, B.; Naghib, S.M.; Younesian, D.; Rabiee, N. Unlocking the rhythmic power of bacterial cellulose: A comprehensive review on green energy harvesting and sustainable applications. *Adv. Funct. Mater.* **2025**, *35*, 2413760. https://doi.org/10.1002/adfm.202413760.
15. Sperotto, G.; Stasiak, L.G.; Godoi, J.P.M.G.; Gabiatti, N.C.; De Souza, S.S. A review of culture media for bacterial cellulose production: Complex, chemically defined and minimal media modulations. *Cellulose* **2021**, *28*, 2649–2673.
16. Xu, Y.; Wei, K.; Bian, L.; Li, G.; Zhang, C. High-yield bacterial cellulose production from rice bran using a genetically characterized *Komagataeibacter europaeus* strain. *Int. J. Biol. Macromol.* **2025**, *310*, 143201. https://doi.org/10.1016/j.ijbiomac.2025.143201.
17. Güzel, M. Valorisation of bread wastes via the bacterial cellulose production. *Biomass Convers. Biorefin.* **2025**, *15*, 4777–4790. https://doi.org/10.1007/s13399-024-05662-7.
18. Esmail, A.; Morais, M.; Yilmazer, U.D.; Neves, L.A.; Freitas, F. Bacterial cellulose production through the valorization of waste apple pulp and stale bread. *Biomass Convers. Biorefin.* **2025**, *15*, 14587–14602. https://doi.org/10.1007/s13399-024-06281-y.
19. Nie, W.; He, Z.; Gu, M.; Zhou, T.; Xu, J.; Zhong, J.; Yang, Y.; Zhong, W. Improved bacterial cellulose production by *Acetobacter oryzoeni* MGC-N8819 in tobacco waste extract coupled with nicotine removal by *Pseudomonas* sp. JY-Q/5Δ. *Int. J. Biol. Macromol.* **2025**, *293*, 139336. https://doi.org/10.1016/j.ijbiomac.2024.139336.
20. Souza, E.F.; Furtado, M. R.; Carvalho, C.W.; Freitas-Silva, O.; Gottschalk, L.M. Production and characterization of *Gluconacetobacter xylinus* bacterial cellulose using cashew apple juice and soybean molasses. *Int. J. Biol. Macromol.* **2020**, *146*, 285–289. https://doi.org/10.1016/j.ijbiomac.2019.12.180.

21. Molina-Ramírez, C.; Enciso, C.; Torres-Taborda, M.; Zuluaga, R.; Gañán, P.; Rojas, O.J.; Castro, C. Effects of alternative energy sources on bacterial cellulose characteristics produced by *Komagataeibacter medellinensis*. *Int. J. Biol. Macromol.* **2018**, *117*, 735–741. https://doi.org/10.1016/j.ijbiomac.2018.05.195.
22. Liu, Z.; Siddique, F.; Wei, Y.; Haque, M.A.; Na, L.; Yang, X.; Lin, C.S.K. Efficient production of bacterial cellulose using *Komagataeibacter sucrofermentans* on sustainable feedstocks. *ChemSusChem* **2025**, *18*, e202401578. https://doi.org/10.1002/cssc.202401578.
23. Mouro, C.; Gomes, A.; Gomes, A.P.; Gouveia, I.C. Sustainable bacterial cellulose production using low-cost fruit wastewater feedstocks. *Nanomaterials* **2025**, *15*, 271. https://doi.org/10.3390/nano15040271.
24. Heydorn, R.L.; Lammers, D.; Gottschling, M.; Dohnt, K. Effect of food industry by-products on bacterial cellulose production and its structural properties. *Cellulose* **2023**, *30*, 4159–4179. https://doi.org/10.1007/s10570-023-05097-9.
25. Liu, Z.; Zhao, R.; Zhang, X.; Wang, H.; Zhang, C.; Liu, J.; Zhu, P. Comparison of bacterial cellulose production by various biomass wastes as culture media. *Int. J. Biol. Macromol.* **2025**, *309*, 143091. https://doi.org/10.1016/j.ijbiomac.2025.143091.
26. Ma, S.; Xi, G.; Feng, X.; Yang, Q.; Peng, Z.; Qiu, D.; Hu, Y.; Zhao, X.; Cheng, L.; Duan, S. Bio-synthesis of bacterial cellulose from ramie textile waste for high-efficiency Cu (II) adsorption. *Sci. Rep.* **2025**, *15*, 18715. https://doi.org/10.1038/s41598-025-02310-6.
27. Lanot, A.; Tiwari, S.; Purnell, P.; Omar, A.M.; Ribul, M.; Upton, D.J.; Eastmond, H.; Badruddin, I.J.; Walker, H.F.; Gatenby, A.; Baurley, S.; Bartolo, P.J.D.S.; Rahatekar, S.S., Bruce, N.C.; McQueen-Mason, S.J. Demonstrating a biobased concept for the production of sustainable bacterial cellulose from mixed textile, agricultural and municipal wastes. *J. Clean. Prod.* **2025**, *486*, 144418. https://doi.org/10.1016/j.jclepro.2024.144418.
28. Salari, M.; Khiabani, M.S.; Mokarram, R.R.; Ghanbarzadeh, B.; Kafil, H.S. Preparation and characterization of cellulose nanocrystals from bacterial cellulose produced in sugar beet molasses and cheese whey media. *Int. J. Biol. Macromol.* **2019**, *122*, 280–288. https://doi.org/10.1016/j.ijbiomac.2018.10.136.
29. Betlej, I.; Rybak, K.; Nowacka, M.; Antczak, A.; Borysiak, S.; Krochmal-Marczak, B.; Lipska, K.; Boruszewski, P. Structural properties of bacterial cellulose film obtained on a substrate containing sweet potato waste. *Crystals* **2022**, *12*, 1191. https://doi.org/10.3390/cryst12091191.
30. Vazquez, A.; Foresti, M.L.; Cerrutti, P., Galvagno, M. Bacterial cellulose from simple and low cost production media by *Gluconacetobacter xylinus*. *J. Polym. Environ.* **2013**, *21*, 545–554. https://doi.org/10.1007/s10924-012-0541-3.
31. Mohammadkazemi, F.; Azin, M.; Ashori, A. Production of bacterial cellulose using different carbon sources and culture media. *Carbohydr. Polym.* **2015**, *117*, 518–523. https://doi.org/10.1016/j.carbpol.2014.10.008.
32. French, A.D. Idealized powder diffraction patterns for cellulose polymorphs. *Cellulose* **2014**, *21*, 885–896. https://doi.org/10.1007/s10570-013-0030-4.
33. French, A.D. Increment in evolution of cellulose crystallinity analysis. *Cellulose* **2020**, *27*, 5445–5448. https://doi.org/10.1007/s10570-020-03172-z.
34. Krichen, F.; Walha, S.; Abdelmouleh, M. Hirshfeld surface analysis of the intermolecular interaction networks in cellulose Iα and Iβ. *Carbohydr. Res.* **2022**, *518*, 108600. https://doi.org/10.1016/j.carres.2022.108600.
35. Gismatulina, Y.A.; Budaeva, V.V.; Kortusov, A.N.; Kashcheyeva, E.I.; Gladysheva, E.K.; Mironova, G.F.; Skiba, E.A.; Shavyrkina, N.A.; Korchagina, A.A.; Zolotukhin, V.N.;Sakovich, G. V. Evaluation of chemical composition of Miscanthus× giganteus raised in different climate regions in Russia. *Plants* **2022**, *11*, 2791.
36. Kashcheyeva, E.I.; Gismatulina, Y.A.; Budaeva, V.V. Pretreatments of non-woody cellulosic feedstocks for bacterial cellulose synthesis. *Polymers* **2019**, *11*, 1645. https://doi.org/10.3390/polym11101645.
37. Miller, G.L. Use of dinitrosalicylic acid reagent for determination of reducing sugar. *Anal. Chem*. **1959**, *31*, 426–428.
38. Dotsenko, A.; Gusakov, A.; Rozhkova, A.; Sinitsyna, O.; Shashkov, I.; Sinitsyn, A. Enzy-matic hydrolysis of cellulosic materi-als using synthetic mixtures of purified cellulases bioengineered at N-glycosylation sites. *3 Biotech* **2018**, *8*, 396. https://doi.org/10.1007/s13205-018-1419-4.
39. Obolenskaya, A.V.; El'nitskaya, Z.P.; Leonovich, A.A. *Laboratornye Raboty po Khimii Drevesiny i Tsellyulozy*; Ekologiya: Moscow, Russia, 1991. (In Russian)
40. Hamed, D.A.; Maghrawy, H.H.; Abdel Kareem, H. Biosynthesis of bacterial cellulose nanofibrils in black tea media by a symbiotic culture of bacteria and yeast isolated from commercial kombucha beverage. *World J. Microbiol. Biotechnol.* **2023**, *39*, 48. https://doi.org/10.1007/s11274-022-03485-0.
41. Gladysheva, E.K.; Skiba, E.A.; Zolotukhin, V.N.; Sakovich, G.V. Study of the Conditions for the Biosynthesis of Bacterial Cellulose by the Producer Medusomyces gisevii Sa-12. *Appl. Biochem. Microbiol.* **2018**, *54*, 179–187. https://doi.org/10.1134/S0003683818020035.

42. Khiabani, A.; Sarabi-Jamab, M.; Pahlevanlo, A.; Shakeri, M.S. Enhancement of Kombucha SCOBY yield through fermentation process optimization: Traditional source vs. alternative substrates. *NFS J.* **2026**, *43*, 100274. https://doi.org/10.1016/j.nfs.2026.100274.
43. Antolak, H.; Piechota, D.; Kucharska, A. Kombucha tea—A double power of bioactive compounds from tea and symbiotic culture of bacteria and yeasts (SCOBY). *Antioxidants* **2021**, *10*, 1541. https://doi.org/10.3390/antiox10101541.
44. Skiba, E.A.; Shavyrkina, N.A.; Skiba, M.A.; Mironova, G.F.; Budaeva, V.V. Biosynthesis of bacterial nanocellulose from low-cost cellulosic feedstocks: Effect of microbial producer. *Int. J. Mol. Sci.* **2023**, *24*, 14401 https://doi.org/10.3390/ijms241814401.
45. Salem, K.S.; Kasera, N.K.; Rahman, M.A.; Jameel, H.; Habibi, Y.; Eichhorn, S.J.; French, A.D.; Pa, L.; Lucia, L.A. Comparison and assessment of methods for cellulose crystallinity determination. *Chem. Soc. Rev.* **2023**, *52*, 6417–6446. https://doi.org/10.1039/d2cs00569g.
46. Kim, U.J.; Eom, S.H.; Wada, M. Thermal decomposition of native cellulose: Influence on crystallite size. *Polym. Degrad. Stab.* **2010**, *95*, 778–781. https://doi.org/10.1016/j.polymdegradstab.2010.02.009.
47. Aleshina, L.A.; Gladysheva, E.K.; Budaeva, V.V.; Mironova, G.F.; Skiba, E.A.; Sakovich, G.V. X-ray diffraction data on the bacterial nanocellulose synthesized by *Komagataeibacter xylinus* B-12429 and B-12431 microbial producers in Miscanthus-and oat hull-derived enzymatic hydrolyzates. *Crystallogr. Rep.* **2022**, *67*, 391–397. https://doi.org/10.1134/S1063774522030026.
48. Torlopov, M.A.; Mikhaylov, V.I.; Udoratina, E.V.; Aleshina, L.A.; Prusskii, A.I.; Tsvetkov, N.V.; Krivoshapkin, P.V. Cellulose nanocrystals with different length-to-diameter ratios extracted from various plants using novel system acetic acid/phosphotungstic acid/octanol-1. *Cellulose* **2018**, *25*, 1031–1046. https://doi.org/10.1007/s10570-017-1624-z.
49. Opdenbosch, D.V. Influences on the accuracy of crystallinities determined by the method of Ruland and Vonk. *Cellulose* **2023**, *30*, 4197–4213. https://doi.org/10.1007/s10570-023-05127-6.
50. Budaeva, V.V.; Korchagina, A.A.; Gismatulina, Y.A.; Kashcheyeva, E.I.; Gorbatova, P.A.; Mironova, G.F.; Zolotukhin, V.N.; Bychin, N.V.; Lyukhanova, I.V.; Aleshina, L.A., Sakovich, G.V. Nitrates of Synthetic Cellulose. *Polymers* **2025**, *18*, 10. https://doi.org/10.3390/polym18010010.
51. Nishiyama, Y.; Sugiyama, J.; Chanzy, H.; Langan, P. Crystal structure and hydrogen bonding system in cellulose Iα from synchrotron X-ray and neutron fiber diffraction. *J. Am. Chem. Soc.* **2003**, *125*, 14300–14306. https://doi.org/10.1021/ja037055w.
52. Nishiyama, Y., Langan, P., Chanzy, H. Crystal structure and hydrogen-bonding system in cellulose Iβ from synchrotron X-ray and neutron fiber diffraction. *J. Am. Chem. Soc.* **2002**, *124*, 9074–9082. https://doi.org/10.1021/ja0257319.
53. ~~47.~~ 53. Lotfy, V.F.; Basta, A.H.; Abdel-Monem, M.O.; Abdel-Hamed, G.Z. Utilization of bacteria in rotten Guava for production of bacterial cellulose from isolated and protein waste. *Carbohydr. Polym. Technol. Appl.* **2021**, *2*, 100076. https://doi.org/10.1016/j.carpta.2021.100076.
54. Jittaut, P.; Hongsachart, P.; Audtarat, S.; Dasri, T. Production and characterization of bacterial cellulose produced by *Gluconacetobacter xylinus* BNKC 19 using agricultural waste products as nutrient source. *Arab. J. Basic Appl. Sci.* **2023**, *30*, 221–230. https://doi.org/10.1080/25765299.2023.2172844.
55. Ghozali, M.; Meliana, Y.; Chalid, M. Synthesis and characterization of bacterial cellulose by *Acetobacter xylinum* using liquid tapioca waste. *Today Proc.* **2021**, *44*, 2131–2134. https://doi.org/10.1016/j.matpr.2020.12.274.
56. Macrae, C.F.; Edgington, P.R.; McCabe, P.; Pidcock, E.; Shields, G.P.; Taylor, R.; Towler, M.; van de Streek J. Mercury: Visualization and analysis of crystal structures. *J. Appl. Cryst.* **2006**, *39*, 453–457. https://doi.org/10.1107/S002188980600731X.
57. Groom, C.R.; Bruno, I.J.; Lightfoot, M.P.; Ward, S.C. The Cambridge Structural Database. *Acta Crystallogr. Sect. B.* **2016**, *72*, 171–179. https://doi.org/10.1107/S2052520616003954.
58. He, F.; Yang, H.; Zeng, L.; Hu, H.; Hu, C. Production and characterization of bacterial cellulose obtained by *Gluconacetobacter xylinus* utilizing the by-products from Baijiu production. *Bioprocess Biosyst. Eng.* **2020**, *43*, 927–936. https://doi.org/10.1007/s00449-020-02289-6.
59. Yilmaz, M.; Goksungur, Y. Optimization of bacterial cellulose production from waste figs by *Komagataeibacter xylinus*. *Fermentation* **2024**, *10*, 466. https://doi.org/10.3390/fermentation10090466.
60. Aleshina, L.A.; Gladysheva, E.K.; Budaeva, V.V.; Skiba, E.A.; Arkharova, N.A.; Sakovich, G.V. X-ray diffraction study of bacterial nanocellulose produced by the *Medusomyces gisevii* Sa-12 culture in enzymatic hydrolysates of oat hulls. *Crystallogr. Rep.* **2018**, *63*, 955–960. https://doi.org/10.1134/S1063774518050024.
61. Bolgova, A.L.; Shevtsov, A.V.; Arkharova, N.A.; Karimov, D.N.; Makarov, I.S.; Gromovykh, T.I.; Klechkovskaya, V.V. Microstructure of gel films of bacterial cellulose synthesized under static conditions of cultivation of the Gluconacetobacter hansenii GH-1/2008 strain on nutrient media with different carbon sources. *Crystallogr. Rep.* **2023**, *68*, 607–614. https://doi.org/10.1134/S1063774523600369.

62. Amorim, J.; Liao, K.; Mandal, A.; Costa, A.F.D.S.; Roumeli, E.; Sarubbo, L.A. Impact of carbon source on bacterial cellulose network architecture and prolonged lidocaine release. *Polymers* **2024**, *16*, 3021. https://doi.org/10.3390/polym16213021.
63. Zeng, X.; Liu, J.; Chen, J.; Wang, Q.; Li, Z.; Wang, H. Screening of the common culture conditions affecting crystallinity of bacterial cellulose. *J. Ind. Microbiol. Biotechnol.* **2011**, *38*, 1993–1999.
64. Aleshina, L.A.; Gladysheva, E.K.; Budaeva, V.V.; Golubev, D.S.; Skiba, E.A.; Sakovich, G.V. X-ray diffraction study of bacterial nanocellulose produced by *Medusomyces gisevii* Sa-12 cultured in enzymatic hydrolysates of miscanthus. *Crystallogr. Rep.* **2019**, *64*, 914–919. https://doi.org/10.1134/S1063774519060026.

Disclaimer/Publisher's Note: The statements, opinions and data contained in all publications are solely those of the individual author(s) and contributor(s) and not of MDPI and/or the editor(s). MDPI and/or the editor(s) disclaim responsibility for any injury to people or property resulting from any ideas, methods, instructions or products referred to in the content.